

# A lucky imaging multiplicity study of exoplanet host stars

C. Ginski<sup>1</sup>\*, M. Mugrauer<sup>1</sup>, M. Seeliger<sup>1</sup>, and T. Eisenbeiss<sup>1</sup>

<sup>1</sup> *Astrophysikalisches Institut und Universitäts-Sternwarte Jena, Jena 07743, Germany*

8 November 2018

## ABSTRACT

To understand the influence of additional wide stellar companions on planet formation, it is necessary to determine the fraction of multiple stellar systems amongst the known extrasolar planet population.

We target recently discovered radial velocity exoplanetary systems observable from the northern hemisphere and with sufficiently high proper motion to detect stellar companions via direct imaging. We utilize the Calar Alto 2.2 m telescope in combination with its lucky imaging camera AstraLux.

71 planet host stars have been observed so far, yielding one new low-mass ( $0.239 \pm 0.022 M_{\odot}$ ) stellar companion, 4.5 arcsec (227 AU of projected separation) northeast of the planet host star HD 185269, detected via astrometry with AstraLux. We also present follow-up astrometry on three previously discovered stellar companions, showing for the first time common proper motion of the 0.5 arcsec companion to HD 126614. Additionally, we determined the achieved detection limits for all targets, which allows us to characterize the detection space of possible further companions of these stars.

**Key words:** techniques: high angular resolution – binaries: close – stars: individual: HD 185269 – stars: individual: HD 126614.

## 1 INTRODUCTION

Recent radial velocity (RV) and transiting exoplanet surveys have resulted in the discovery of a large number of new exoplanetary systems. Most stars are born in binary or multiple systems (Mathieu et al. 2000, Duchêne et al. 2007), and indeed we observe that a reasonable fraction of the stars in the Galaxy are multiple (Lada 2006). The effects of additional stellar companions on the planet formation process are therefore of high interest to constrain and calibrate planet formation theories.

A number of studies have been conducted on this subject in the past, such as described in Mugrauer et al. (2007) or Daemgen et al. (2009) and most recently in Röll et al. (2011) and Chauvin et al. (2011). As a result of these studies, 43 multiple stellar systems hosting exoplanets are known to date, suggesting that about 17 % of all known exoplanets reside in such systems (Mugrauer et al. 2009).

In this paper we present the results of our ongoing multiplicity study of the most recently (since 2008) discovered RV exoplanet host stars. We utilized the Calar Alto 2.2 m telescope and the AstraLux instrument (Hormuth et al. 2008) to achieve imaging data with higher Strehl ratio compared to simple seeing-limited imaging.

In the following section we characterize our sample. In sec-

tion 3 we give a brief introduction to the observation technique as well as the instrument used and describe the reduction and astrometric calibration of our data. In section 4 we show all confirmed or rejected companion candidates with the associated proper motion analysis. We also present detection limits for all studied systems. Finally in section 5 we summarize our findings.

## 2 TARGET SAMPLE

Our sample consists of stars with RV planet candidates discovered between 2008 and 2011. They are all observable from the northern hemisphere with declinations down to  $-22^{\circ}$  and a relatively even distribution in right ascension. Since we want to test companionship of detected companion candidates via astrometry, we chose targets which are close enough to show a sufficient proper motion (e.g.  $> 47$  mas/yr or approximately one Astralux pixel per year) to do a common proper motion analysis approximately one year after the first epoch images were taken. The distance distribution of our targets is shown in Fig. 1. On average our targets are 56.6 pc away and show a proper motion of 180.4 mas/yr equivalent to 3.8 pix/yr on the Astralux instrument.

The RV planet search technique favors main-sequence stars, therefore the average age of our target stars is 4.6 Gyr (data as listed in exoplanet.eu by Schneider et al. 2011). Spectral types range from late F to early M, with the majority being

\* E-mail:ginski@astro.uni-jena.de

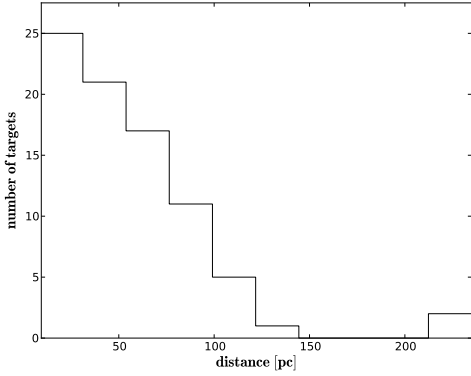


**Figure 1.** Histogram of distances of all our target stars (as listed in exoplanet.eu by Schneider et al. 2011). The majority being within 100 pc.

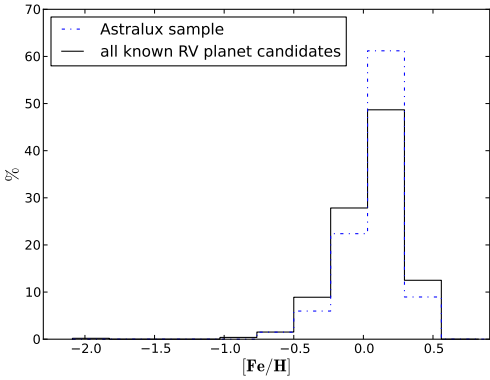


**Figure 2.** Metallicity distribution for all targets in our sample. For comparison we plot the metallicity distribution of all RV planet candidate host stars discovered so far (as listed in exoplanet.eu by Schneider et al. 2011).

G and K type. In Fig. 2 we show the metallicity distribution of our sample compared to the whole RV planet candidate host population. The average metallicity of our sample is slightly higher than solar metallicity at 0.09. The metallicity distribution of our sample does not differ significantly from the whole population.

In Fig. 3 we present the minimum masses of detected RV planet candidates versus their semi-major axis for our sample and the whole population. The majority of the detected planet candidates are located within 2 AU of their hosts. The average minimum mass of our sample is  $2.8 M_{Jup}$ , as compared to  $2.4 M_{Jup}$  for the whole RV planet candidate population. Given the standard deviation of  $3.3 M_{Jup}$  and  $3.8 M_{Jup}$  respectively this is not significant.

The eccentricity distribution of RV planets around our sample stars can be seen in Fig. 4. We compared the eccentricity distribution of our sample to that of all RV planet candidates and found no significant differences.

We conclude that the general properties of our sample resemble those of the whole population.

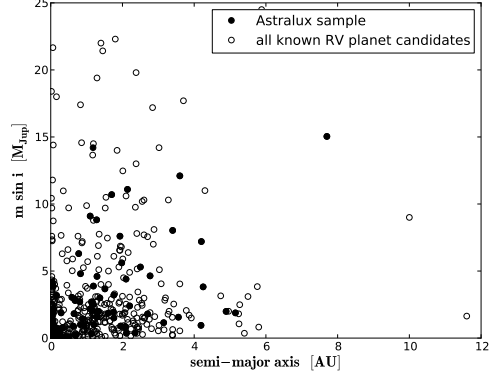


**Figure 3.** Minimum mass versus separation for all planet candidates orbiting hosts included in our sample (as listed in exoplanet.eu by Schneider et al. 2011). For comparison we also plot minimum mass versus separation of all RV planet candidates discovered so far.

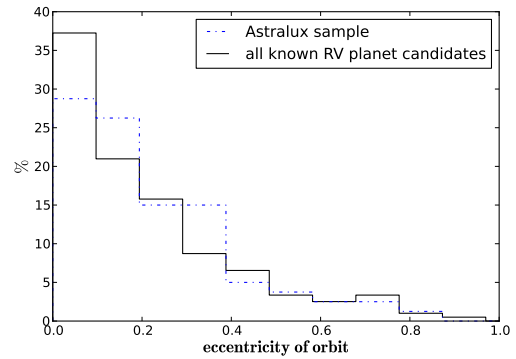


**Figure 4.** Eccentricity distribution of planet candidates orbiting hosts included in our sample. For comparison we also plot the eccentricity distribution of all RV planet candidates discovered so far (as listed in exoplanet.eu by Schneider et al. 2011).

### 3 OBSERVATIONS OUTLINE AND DATA CALIBRATION

#### 3.1 Lucky imaging technique

To achieve high spatial resolution as well as high sensitivity, one must consider the effects of turbulent atmosphere. Given the Rayleigh criterion for the minimum resolvable angle of  $\Theta = 1.22 \cdot \lambda \cdot D^{-1}$ , the Calar Alto 2.2m telescope has a theoretical resolution of 89 mas at a wavelength of 776 nm, which is the central wavelength of the SDSS  $i'$  filter which we are using. The median seeing at the Calar Alto site, however, is 0.9 arcsec (Sánchez et al. 2007), which is about 10 times larger.

The atmospheric conditions in the optical regime are subject to rapid variations with a timescale that can be approximated by the speckle coherence time  $\tau_e \approx 0.36 \cdot r_0 \cdot \Delta\nu^{-1}$  (Roddier et al. 1982), where  $r_0$  is the Fried-parameter and  $\Delta\nu$  is the wind speed dispersion in the atmosphere. For a typical wind speed dispersion of  $\Delta\nu \approx 10 \text{ m} \cdot \text{s}^{-1}$  at the Calar Alto site and a V-band seeing of 0.7 arcsec,  $\tau_e$  is in the order of 100 ms (Hormuth, Diploma Thesis 2007). Within  $\tau_e$  the

resulting speckle pattern will remain fixed, whereas longer integration times would lead to an averaged and therefore "smeared out" speckle pattern.

The lucky imaging approach consists of taking several thousand short images with integration times shorter than  $\tau_e$ , to sample the speckle variations during the observation window. We then only choose the so called "lucky shots" with a very high Strehl ratio in one of the speckles, to shift and add, resulting in a final image with the highest possible strehl ratio and therefore highest possible angular resolution.

For an in-depth introduction to the lucky imaging technique please see Law et al. (2006).

### 3.2 Observations and data reduction

All observations were carried out with the Calar Alto 2.2 m telescope in combination with the AstraLux instrument. This instrument consists of a back-illuminated, electron-multiplying, frame transfer CCD, which is well suited for the lucky imaging observation technique. For a detailed description of the instrument, see Hormuth et al. (2008).

Since we wanted to detect low-mass stellar or even brown dwarf companions of our targets, we chose the SDSS  $i'$  filter as described in Fukugita et al. (1996) for all observations. This is the best choice taking into account the sensitivity of the detector and the brightness of the detectable companions, as well as the variability of the atmosphere. For calibration we took dome- and sky-flats at the beginning and/or end of each observation night.

For all science targets we chose 29.54 ms of exposure time per frame, which is well below the typical speckle coherence time at the Calar Alto site. Shorter exposure times would have led to significantly growing overheads since we would have needed to switch off the frame transfer mode of the instrument. Longer exposure times would have resulted in a less localized and more "smeared out" speckle pattern.

The electron-multiplying gain was individually adjusted for each target to obtain the maximum signal while still operating in the linear regime of the detector. We then took 100 dark frames with closed shutter and with the respective electron multiplying settings before the start of each acquisition sequence.

Depending on weather conditions and time constraints we took between 10000 and 80000 frames per science target, which corresponds to a total integration time of 0.25 min and 1.97 min respectively for a typical frame selection rate of 5 %. The obtained AstraLux images are all reduced and processed with our own ESO-MIDAS (Munich Image Data Analysis System) software for the reduction of imaging data taken with the lucky imaging technique. The individual AstraLux images are dark-subtracted with the median (for optimal suppression of cosmic ray artifacts) of several short integrated dark-frames and flat-fielded. For the lucky imaging data processing, the reached Strehl-Ratio in all individual images is determined at first using the bright planet host star as Strehl-probe. The frames are then ranked according to their Strehl-Ratio and only the best 10, 5, and 1 % of all frames, i.e. only the frames with the highest Strehl-Ratio, are then selected and combined using the shift+add technique. Thereby, for image registration, the position of the brightest pixel in the speckle pattern of the planet host

**Table 1.** Hipparcos astrometry of epoch 1991.25 of our calibration binaries

Binary	Separation [arcsec]	Position Angle [°]
HIP 59585	$18.677 \pm 0.032$	$190.83 \pm 0.10$
HIP 65205	$15.041 \pm 0.015$	$219.44 \pm 0.06$
HIP 67099	$18.751 \pm 0.028$	$343.33 \pm 0.09$
HIP 72508	$15.248 \pm 0.014$	$91.36 \pm 0.05$
HIP 80953	$16.356 \pm 0.021$	$195.69 \pm 0.07$

**Table 2.** Astrometric calibration of all observation epochs. We list the pixel-scale (PS) and the position angle (PA) of the y-axis for all observation epochs.

Epoch	PS [mas/pix]	PA of y-axis [°]
23/04/2008	$47.278 \pm 0.101$	$0.17 \pm 0.23$
11/07/2008	$47.180 \pm 0.078$	$0.44 \pm 0.15$
16/01/2009	$47.237 \pm 0.114$	$359.39 \pm 0.08$
07/09/2009	$47.220 \pm 0.100$	$0.43 \pm 0.13$
23/02/2010	- <sup>1</sup>	- <sup>1</sup>
14/07/2010	$47.243 \pm 0.049$	$358.49 \pm 0.22$
14/01/2011	$47.365 \pm 0.135$	$358.07 \pm 0.12$
27/07/2011	$47.160 \pm 0.066$	$358.37 \pm 0.23$

<sup>1</sup> due to bad weather conditions no astrometric calibrators could be observed

star is determined in all frames, which are then shifted and averaged.

### 3.3 Astrometric calibration

Since we want to precisely measure separation and position angle of our companion candidates with respect to the primary stars, and the AstraLux instrument is not permanently mounted to the Calar Alto 2.2m telescope, a careful astrometric calibration of the detector in each observation epoch is necessary. For this purpose we selected a sample of five wide binaries, for which precise Hipparcos measurements as well as several additional observation epochs are available. We show our sample along with the Hipparcos astrometry in Table 1. Furthermore, we observed the center of the globular cluster M15 whenever possible, for which precise HST astrometry is available.

For each epoch we have a minimum of three calibrators which were observed in the same night as the science targets. For all calibrators we used the Hipparcos measurement of epoch 1991.25 as reference point and then linearly fitted the slow orbital motion by using all data points available in the Washington Double Star (WDS) catalog.

The pixel scales and position angles of the calibration images for each individual calibrator were calculated using ESO-MIDAS for the position measurements of the binary components, and GAIA (Graphical Astronomy and Image Analysis Tool) for the respective measurements of the M15 cluster components (using SExtractor: Software for source extraction by Bertin and Arnouts 1996). The average of these calculations were used as final calibration for the respective epoch to cancel out systematic errors due to residual orbital motion of our binary stars. The final astrometric calibrations for all observation epochs are listed in Table 2.

### 3.4 PSF subtraction and astrometric measurements

Since we are searching for faint low-mass stellar companions to bright stars, we subtract the primary stars' PSF in order to detect the companions with highest possible signal-to-noise. Due to the random nature of the lucky imaging approach, the PSFs in the final reduced images may vary significantly from star to star, for example as a function of the average zenith distance of the observed objects. Hence it is not feasible to subtract a PSF standard from all the images. Furthermore, the PSFs of our target stars are not necessarily symmetrical in nature, rendering simple rotation subtraction techniques ineffective.

Given these limitations, we found the best approach to be an unsharp mask filter. We fold the images with a 2-dimensional Gaussian of size  $n$  to "blur" them, and then subtract the "blurred" images from the originals, thus eliminating all low spatial frequencies from the images. We tested sizes  $n$  between 5 and 20 pixels for different images, with  $n = 10$  generally yielding the best results in terms of improving the signal-to-noise of the faint companion candidates.

We again used ESO-MIDAS for all astrometric measurements, first measuring the primary star's position in the original images, then applying the PSF subtraction as described, before measuring the companion candidate's position. We always measured both positions multiple times, averaging the results to avoid statistical errors.

## 4 RESULTS

To date we observed 71 planet host-stars in our project. In seven cases we detected faint companion candidates, of which three were already known. In the following paragraphs, we show the astrometric measurements for all the companion candidates, as well as the proper motion analysis, to determine which of the objects are physically associated to the target stars.

### 4.1 Imaging of known companions

In the course of our study we imaged three already known companions to exoplanet hosts, to test the instrument capabilities and to provide additional astrometric measurements for future orbit solutions. The final reduced images can be seen in Fig. 5 and our astrometric measurements are listed in Table 3.

The stellar companion to  $\tau$  Boo resides at an angular separation  $2.181 \pm 0.018$  arcsec, which corresponds to a projected separation of 34 AU. Patience et al. (2002) stated, that  $\tau$  Boo A and B form an eccentric binary system with a semi-major axis of  $\approx 225$  AU, and masses of  $\approx 1.3 M_{\odot}$  and  $\approx 0.4 M_{\odot}$  respectively.

HD 176051 A and B form a close binary system of only  $1.139 \pm 0.009$  arcsec separation and an orbital period of 61.2 yr. The stellar masses are  $1.07 M_{\odot}$  and  $0.71 M_{\odot}$  respectively (Muterspaugh et al. 2010). Muterspaugh et al. (2010) found an astrometric companion of  $\approx 1.5 M_J$ , to be orbiting one of the components.

The stellar companion to HD 126614 was only detected recently by Howard et al. (2010) at the Palomar Observa-

**Table 3.** Astrometric measurements of all known companions

Primary	Epoch	Separation [arcsec]	Position Angle [ $^{\circ}$ ]
$\tau$ Boo	23/04/2008	$2.181 \pm 0.011$	$46.26 \pm 0.42$
HD 176051	27/07/2011	$1.139 \pm 0.005$	$252.12 \pm 0.40$
HD 126614	14/01/2011	$0.499 \pm 0.067$	$60.70 \pm 5.60$

tory, using adaptive optics imaging. It is separated from the primary only by  $0.490 \pm 0.051$  arcsec, which corresponds to a projected separation of 35.6 AU. The mass of the companion was inferred from the JHK photometry, to be  $0.324 \pm 0.004 M_{\odot}$ . Its companionship was so far only confirmed by photometry and radial velocity trend. We are not aware of any further observations of this companion, especially regarding whether or not it is actually co-moving with the primary. Hence we present a proper motion analysis in section 4.3, using the measurements by Howard et al. (2010) and our own AstraLux data point, to confirm that HD 126614 A and B form indeed a common proper motion pair.

### 4.2 New companion candidates

In the course of our study we found new faint companion candidates around the planet host stars HD 185269, HD 183263, HD 187123 and HD 13931. In Fig. 6 we show the epochs with the highest signal-to-noise.

In Table 4 we show all the astrometric measurements obtained in the different observation epochs for all companion candidates. Given the distances of the primary stars, the detected objects would have projected separations ranging from 179 AU (close candidate of HD 187123) up to 781 AU (far candidate of HD 187123).

### 4.3 Proper motion analysis

We performed a proper motion analysis for all companion candidates listed in Table 4 to distinguish between true physical companions and distant background objects. Hence we computed how separation and position angle would change from the first to the last observation epoch if the detected objects are indeed only in the background, and are therefore most likely standing still, also considering the effect of the annual parallax due to the earth's motion around the sun. We then compared these expected positions with the actual positions measured in our images. The resulting diagrams for all new companion candidates are listed in Fig. 7. Even if the detected objects are physically associated to the primaries, they might show a slightly different proper motion, which can be explained by orbital motion around the primary star. To account for this, we also added to the analysis the maximum possible change of separation and position angle due to orbital motion at the projected distance of our first epoch measurement. We assumed an edge-on circular orbit for changes in separation and a face-on circular orbit for changes in position angle respectively.

HD 13931



**Figure 5.** Follow-up images of already known companions to exoplanet host stars taken in SDSS  $i'$  filter during our ongoing campaign. All images have been PSF subtracted. North is always up and east to the left. The companions are marked by arrows.

**Table 4.** Astrometric measurements of all companion candidates

Primary	Epoch	# CC	Separation [arcsec]	Position Angle [°]
HD 13931	14/01/2011	1	$9.972 \pm 0.030$	$19.50 \pm 0.16$
	27/07/2011	1	$10.003 \pm 0.015$	$19.16 \pm 0.25$
HD 185269	07/09/2009	1	$4.522 \pm 0.014$	$7.91 \pm 0.23$
	14/07/2010	1	$4.520 \pm 0.010$	$8.17 \pm 0.30$
	27/07/2011	1	$4.511 \pm 0.008$	$8.44 \pm 0.28$
HD 183263	23/04/2008	1	$14.190 \pm 0.032$	$47.83 \pm 0.26$
		2	$3.295 \pm 0.015$	$349.55 \pm 0.40$
	11/07/2008	1	$14.183 \pm 0.028$	$47.92 \pm 0.19$
		2	$3.245 \pm 0.017^1$	$349.72 \pm 0.31^1$
	07/09/2009	1	$14.244 \pm 0.033$	$47.93 \pm 0.17$
		2	$3.315 \pm 0.031$	$350.75 \pm 0.56$
HD 187123	11/07/2008	1	$2.926 \pm 0.011$	$48.11 \pm 0.29$
		2	$11.560 \pm 0.022$	$263.12 \pm 0.19$
	07/09/2009	1	$2.917 \pm 0.013$	$43.92 \pm 0.29$
		2	$11.696 \pm 0.028$	$263.92 \pm 0.17$

<sup>1</sup> due to the spurious detection of the companion candidate this data point seems dubious

HD 13931 was observed in January and July 2011. The associated proper motion plot can be found in Fig. 7(a). The data point taken in July 2011 is, within its uncertainty, consistent with the background and common proper motion hypothesis. The common proper motion hypothesis can be rejected only on the  $0.83$  and  $1.09\sigma$  level for separation and position angle respectively, hence it is not possible to draw a final conclusion from our AstraLux measurements.

This companion candidate was resolved in 2MASS (Two Micron All Sky Survey) J, H and Ks-band images taken on October 28th 1998. We show the corresponding Ks-band image in Fig. 8. Our measurements for this epoch yield a separation of  $8.13 \pm 0.15$  arcsec and a position angle of  $31.14^\circ \pm 0.75^\circ$ . Using this new data point, we created a proper motion plot as shown in Fig. 9. Although the 2MASS data points are not consistent with the background hypothesis within  $1\sigma$ , we can still reject common proper motion with  $10.38\sigma$  for separation and  $11.29\sigma$  for position angle. The inconsistency with the background hypothesis is most likely caused by a slow proper motion of the detected object. We conclude that our companion candidate around

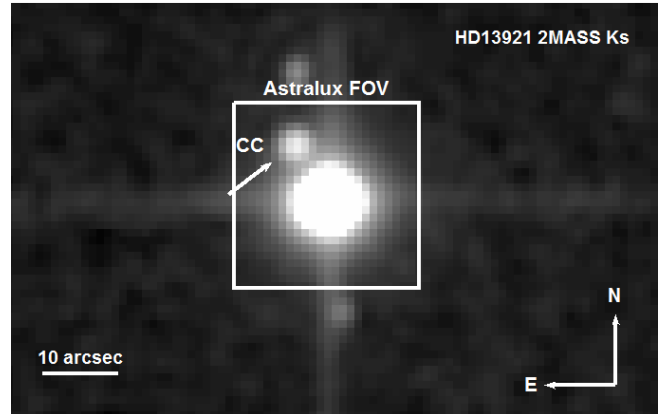


**Figure 8.** 2MASS Ks-Band Image of HD 13931 in epoch 28/10/1998. The AstraLux field of view is indicated by the white rectangle.

HD 13931 is only a background object.

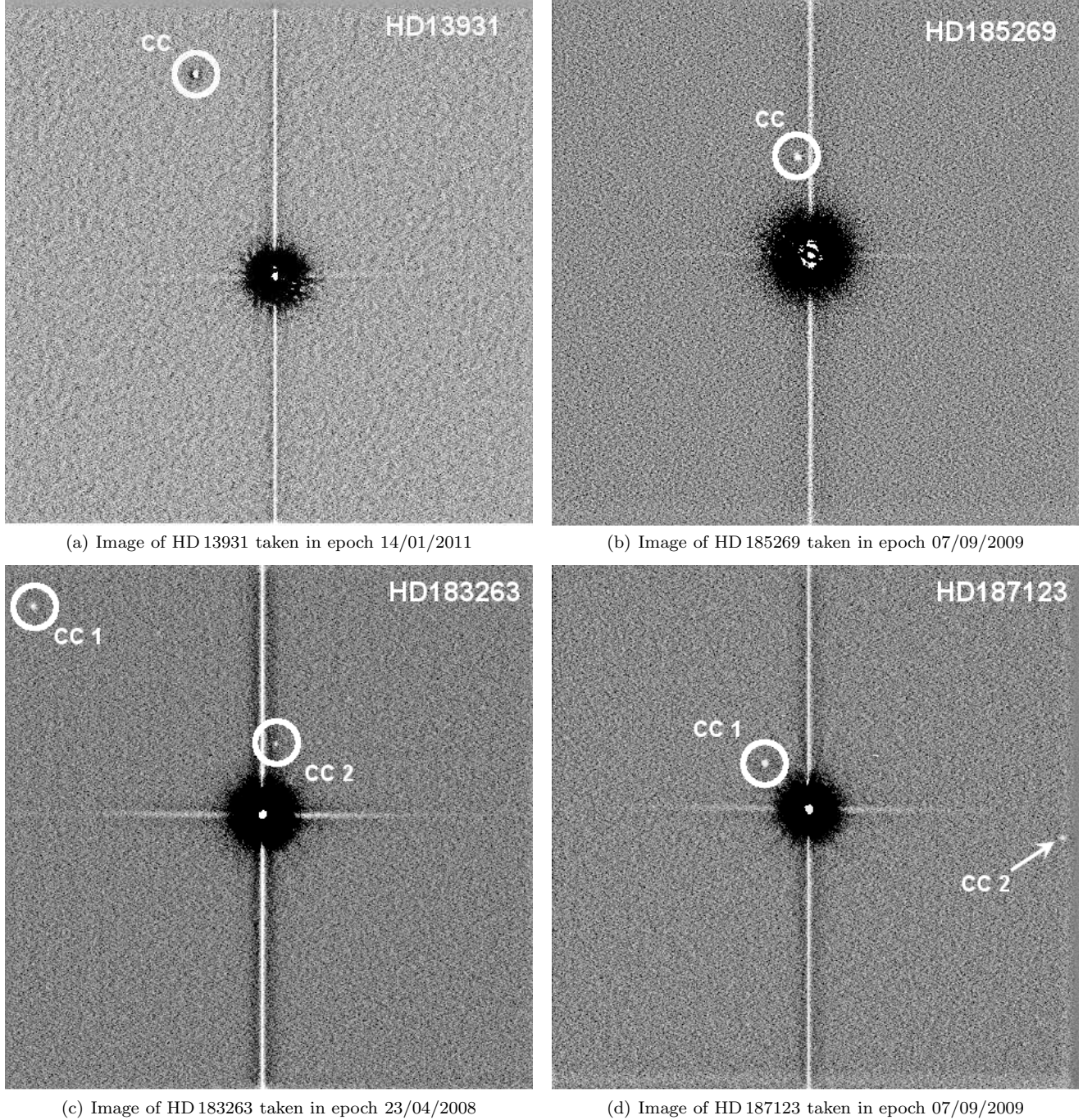


**Figure 6.** Images of our newly discovered companion candidates taken in SDSS  $i'$  filter. Images are  $24.2 \times 24.2$  arcsec, north is always up and east to the left. In all cases the primary stars PSF was subtracted by an unsharp mask filter. Companion candidates are marked with circles and arrows. The numbers assigned to multiple companion candidates match those used in Table 4.

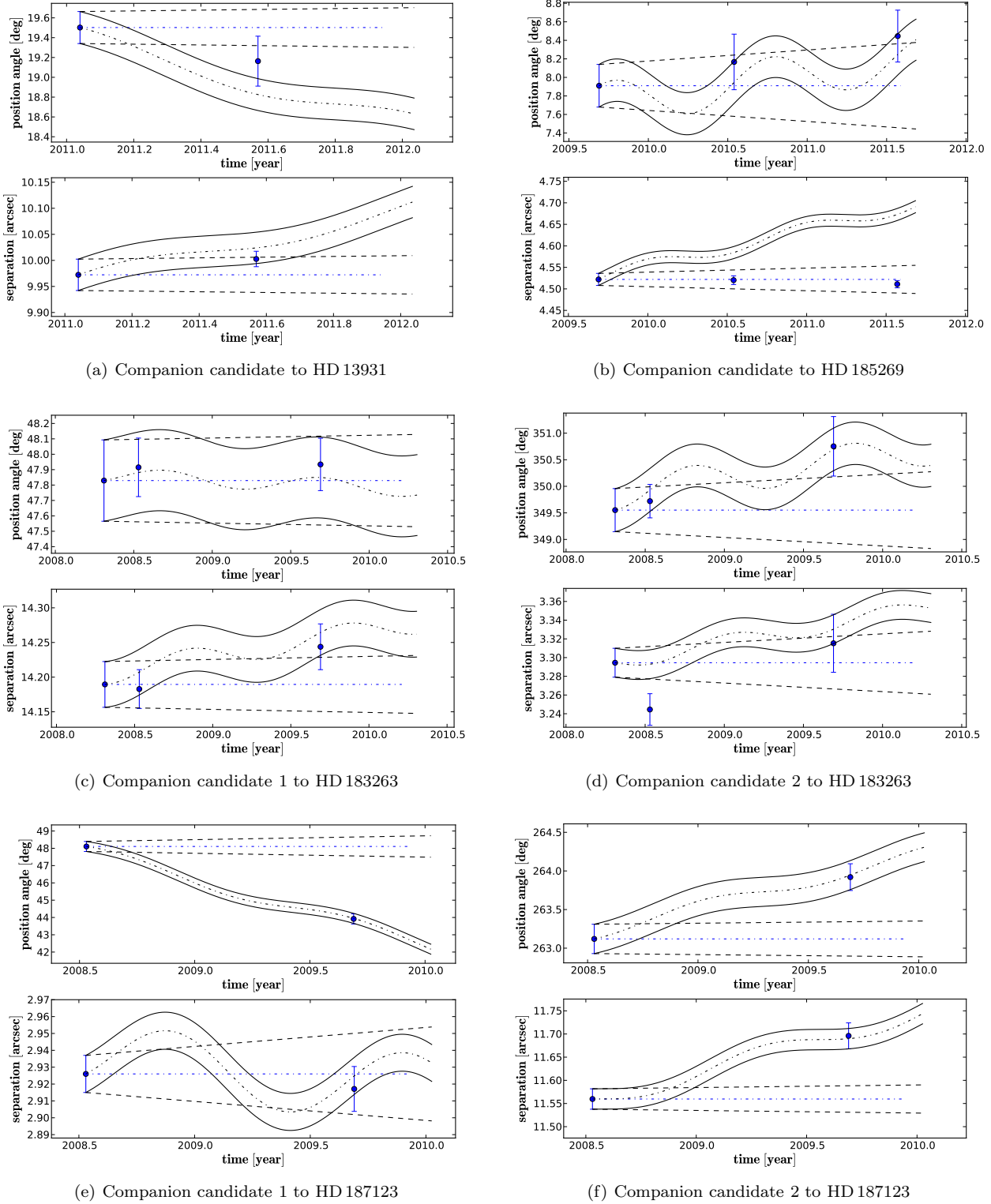


**Figure 7.** Proper motion diagrams for all newly discovered companion candidates. Upper diagrams are always for the position angle and lower diagrams for the separation, both plotted over time in years. The dashed lines mark the area for maximum possible orbital motion in case of bound objects and circular orbits. The solid lines mark the area for non-moving background objects. The wobble in the background hypothesis is introduced by the annual parallax.

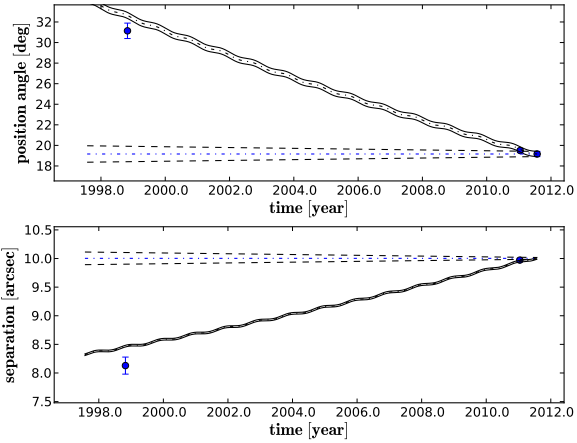


**Figure 9.** Proper motion diagram for the companion candidate to HD 13931 including a 2MASS measurement of epoch 28/10/1998. The areas for maximum orbital motion and background hypothesis are plotted backwards from our latest measurement in epoch 27/07/2011.

#### HD 185269

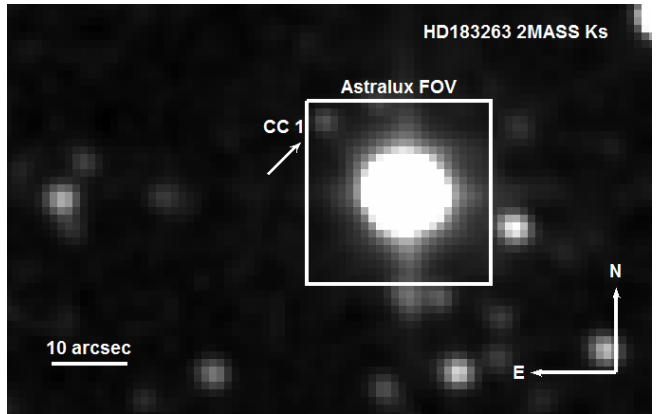
In Fig. 7(b) we show the proper motion plot for the companion candidate next to HD 185269. Due to the overlap of background and common proper motion area in the position angle plot, our angular measurements would be consistent with both hypothesis. However, our measurements of the separation are only consistent with an object of common proper motion with the primary star. We can reject the background hypothesis with  $9.9\sigma$ , and are therefore concluding that our object is indeed a previously unknown stellar companion to HD 185269. HD 185269 B has a projected separation of 227 AU. Further follow-up observations will be executed to determine the orbital motion of the B component.

Using IRAF (Image Reduction and Analysis Facility) standard aperture photometry, we calculate an average magnitude difference of  $\Delta I = 7.2 \pm 0.2$  mag throughout all our observation epochs. Given the age of the primary of 4.2 Gyr (Johnson et al. 2006) and the parallax of  $21.11 \pm 0.74$  mas (van Leeuwen 2007), we find a mass of  $0.239 \pm 0.022 M_\odot$ , using the models by Baraffe et al. (1998).

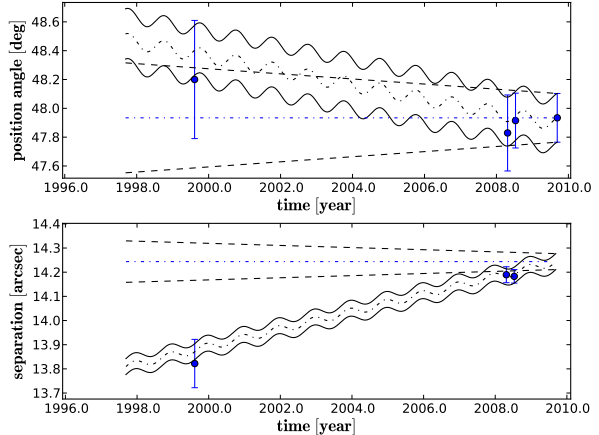
#### HD 183263

Fig. 7(c) and 7(d) show the proper motion plots for the two companion candidates discovered around HD 183263.

Due to the comparatively small proper motion of only  $38.09 \text{ mas}\cdot\text{yr}^{-1}$  ( $\approx 0.8$  AstraLux pix), a final conclusion for the first companion candidate is difficult with our epoch difference of 1.25 yr. The position angle gives no useful information, since the background and common proper motion area are completely overlapping, and we can only reject the common proper motion hypothesis with  $1.06\sigma$ , in the case of the separation. We could, however, identify our first companion candidate once more in the 2MASS catalogue. We show the corresponding image in Ks-band in Fig. 10. The image was taken on August 5th 1999, giving us 10 yr of epoch difference. The 2MASS-PSC



**Figure 10.** 2MASS Ks-Band Image of HD 183263 in epoch 05/08/1999. The Astralux field of view is indicated by the white rectangle.



**Figure 11.** Proper motion diagram for the first (far) companion candidate to HD 183263 including a 2MASS measurement of epoch 08/1999. The areas for maximum orbital motion and background hypothesis are plotted backwards from our latest measurement in epoch 07/09/2009.

(2MASS - Point Source Catalogue, Cutri et al. 2003) measurements yield a separation of  $13.8 \pm 0.1$  arcsec and a position angle of  $48.2^\circ \pm 0.4^\circ$ . Using this information, we created a new proper motion plot incorporating the 2MASS epoch which is shown in Fig. 11. Even though the error bars are significantly larger than the ones of our Astralux measurements, the new proper motion analysis in separation clearly indicates that the first companion candidate around HD 183263 is a background object, with a significance of  $3.3\sigma$ .

The second (closer) companion candidate was also detected in all three observation epochs. In July 2008 it was only barely visible, making these data points somewhat dubious. While the separation measurements are in general still consistent with a co-moving object as well as a background object, the development of the position angle indicates (with  $1.4\sigma$  corresponding to 83.8% probability) that the second companion candidate is a background object as well.

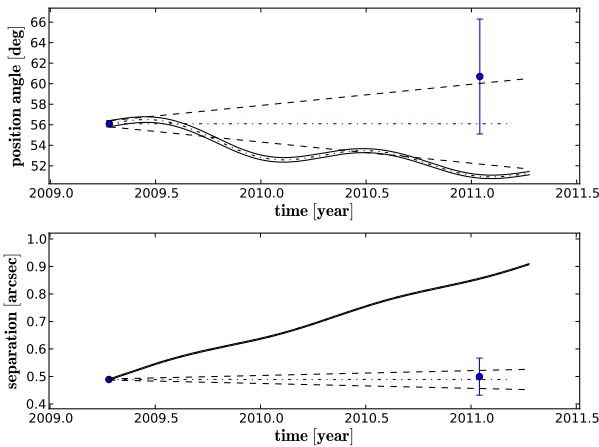


**Figure 12.** Proper motion diagrams for the stellar companion to HD 126614

#### HD 187123

The proper motion plots for the two companion candidates around HD 187123 are shown in Fig. 7(e) and 7(f). Both companion candidates show as fully consistent with the background hypothesis with an average significance level of  $3.3\sigma$ . We conclude that both objects are indeed distant, non-moving background objects. HD 187123 is a single star within the given detection limits described in section 4.4.

#### HD 126614

We also performed a proper motion analysis for the companion to HD 126614, using the measurements by Howard et al. (2010) as first epoch, and our own AstraLux measurement as second epoch. The resulting plot is shown in Fig. 12.

Our measured separation of  $499 \pm 67$  mas and position angle of  $60.7^\circ \pm 5.6^\circ$  are consistent with the the astrometry of the companion in the discovery epoch ( $489.0 \pm 1.9$  mas and  $56.1^\circ \pm 0.3^\circ$ , as given by Howard et al. 2010). However, due to the very low declination of  $-05^\circ 10' 4''$ , we had to observe HD 126614 at high air mass, which led to an extended PSF in north-south direction. This made it very difficult to determine the position angle precisely, which is also evident in the large error bars of the measurement. Still the position angle is, within its error bars, consistent with common proper motion.

Despite the uncertainties in the position angle, we can still reject the background hypothesis with  $1.7\sigma$  and  $5.3\sigma$  for position angle and separation respectively. We can therefore conclude that HD 126614 B is indeed physically associated with A.

Due to the small separation between primary and companion, aperture photometry with IRAF is not viable. We could, however, infer the I-band magnitude difference of companion and primary from the ratio of the peak counts. We calculate  $\Delta I = 5.59 \pm 0.15$  mag. Given the  $\log(\text{age}) = 9.1$  (Howard et al. 2010) and parallax of  $14.63 \pm 1.15$  mas (van Leeuwen 2007), we find a mass of  $0.307 \pm 0.033 M_\odot$ , using the models by Baraffe et al. (1998).

This is consistent with the mass of  $0.324 \pm 0.004$  found by Howard et al. (2010).

#### 4.4 Detection limits and non-detections

In Table 6 and Table 7 we list all the systems that were observed in our survey to date, with and without additional stellar components detected, respectively. We also list the epochs in which these systems have been observed, since our detection limits vary with the weather and seeing conditions. Additionally we present limits for the lowest mass objects detectable at separations of 0.5, 1, 2 and 5 arcsec, at a signal-to-noise ratio of 5, in the PSF subtracted images. We calculated the uncertainties of these mass limits considering the uncertainties in the measured parallaxes for each system, as well as a maximum photometric error of 0.2 mag in our AstraLux images, along with an average photometric error of 0.05 mag in the primary stars' I-band magnitudes. In Fig. 13 we show the average dynamic range plots for each of our observation epochs. We determined the average dynamic range by measuring the noise levels in all reduced images of a given epoch with a frame selection rate of 5 %, assuming a signal-to-noise ratio of 5. The primary stars' PSF was always subtracted to get the best possible results.

In all but two epochs we reach a magnitude difference of  $\Delta I = 10$  mag outside of 2 arcsec from the primary star. Given the average absolute magnitudes and ages of the target stars in each epoch as listed in Table 5 (calculated from individual values as listed in Simbad and exoplanet.eu respectively), and using the models by Baraffe et al. (1998), we would have easily been able to detect all wide stellar companions. Furthermore, we still probe the low mass stellar regime ( $M < 0.15 M_\odot$ ) down to separations of 1 arcsec from the primary star.

The observation epochs in January 2009 and February 2010 suffered from bad weather conditions, and while we could complete most of our observation program in January 2009, we could only observe for approximately one hour through the cloud cover in February 2010. This is reflected in the dynamic range graphs 13(c) and 13(e), which show a noticeable decline in sensitivity in comparison with the other observation epochs. On average we are still able to detect stellar companions down to  $0.15 M_\odot$  outside of 1.2 arcsec and 3.1 arcsec respectively.

If we average all minimum masses for the respective separations as derived in Table 7, we conservatively get detection limits of  $0.34 M_\odot$  at 0.5 arcsec as well as  $0.22 M_\odot$  at 1 arcsec and  $0.15 M_\odot$  outside of 2 arcsec. Given our field of view, we can detect such low-mass stellar companions up to separations of 12 arcsec.

## 5 CONCLUSIONS

In our ongoing study we observed 71 planet host stars to date. Of these 71 systems, 3 were already known to be multiple, for which we present follow up astrometry. Thereby, we show for the first time conclusively, that the companion to HD 126614 is indeed physically associated with the primary. As the planet host star HD 126614 also exhibits a further companion at a wider separation (HD 216614 C, sep =  $41.914 \pm 0.110$  arcsec (3043 AU), PA =  $299.36^\circ \pm 0.14^\circ$

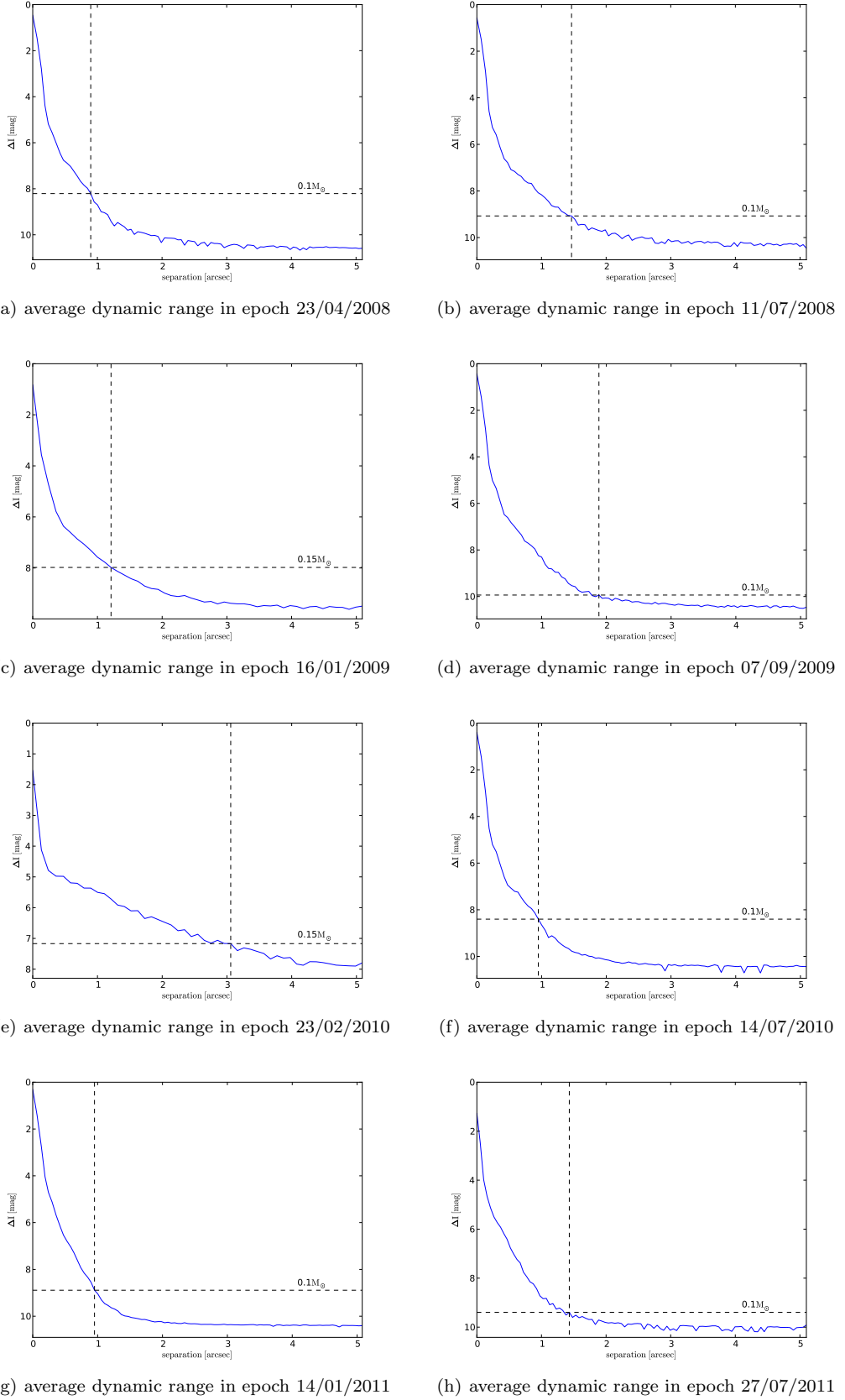


**Figure 13.** Average dynamic range plots for a signal-to-noise of 5 for all our observation epochs. The dashed lines represent the detectable minimum mass objects at a given separation from the primary star, using the model by Baraffe et al. (1998). The primary stars' PSF was always subtracted by unsharp mask filtering before determining the dynamic range.

**Table 6.** List of all stars with companions and companion candidates detected. We give the numbers of frames observed, each frame with an exposure time of 29.54 ms. We also give an upper limit for the minimum mass detectable at 0.5, 1, 2 and 5 arcsec using the models by Baraffe et al. (1998) and assuming an average age for each epoch as listed in Table 5.

Star	Epoch	# of frames	M [ $M_{\odot}$ ] at 0.5''	M [ $M_{\odot}$ ] at 1''	M [ $M_{\odot}$ ] at 2''	M [ $M_{\odot}$ ] at 5''
HD13931	14/01/2011	50000	0.173 $\pm$ 0.014	0.097 $\pm$ 0.003	0.086 $\pm$ 0.001	0.085 $\pm$ 0.001
	27/07/2011	50000	0.365 $\pm$ 0.036	0.142 $\pm$ 0.010	0.105 $\pm$ 0.004	0.100 $\pm$ 0.004
HD183263	23/04/2008	50000	0.194 $\pm$ 0.020	0.099 $\pm$ 0.003	0.086 $\pm$ 0.001	0.085 $\pm$ 0.001
	11/07/2008	80000	0.180 $\pm$ 0.016	0.144 $\pm$ 0.011	0.099 $\pm$ 0.003	0.088 $\pm$ 0.002
	07/09/2009	80000	0.178 $\pm$ 0.015	0.096 $\pm$ 0.003	0.087 $\pm$ 0.001	0.086 $\pm$ 0.002
HD187123	11/07/2008	77800	0.149 $\pm$ 0.010	0.103 $\pm$ 0.004	0.086 $\pm$ 0.001	0.083 $\pm$ 0.001
	07/09/2009	80000	0.160 $\pm$ 0.012	0.091 $\pm$ 0.002	0.084 $\pm$ 0.001	0.084 $\pm$ 0.001
	07/09/2009	50000	0.307 $\pm$ 0.032	0.166 $\pm$ 0.013	0.107 $\pm$ 0.005	0.096 $\pm$ 0.003
HD185269	14/07/2010	60000	0.286 $\pm$ 0.027	0.125 $\pm$ 0.007	0.093 $\pm$ 0.003	0.091 $\pm$ 0.002
	27/07/2011	50000	0.239 $\pm$ 0.021	0.113 $\pm$ 0.006	0.091 $\pm$ 0.002	0.089 $\pm$ 0.002
$\tau$ Boo	23/04/2008	50000	0.208 $\pm$ 0.019	0.104 $\pm$ 0.004	0.088 $\pm$ 0.001	0.088 $\pm$ 0.001
HD176051	27/07/2011	50000	0.149 $\pm$ 0.010	0.095 $\pm$ 0.003	0.084 $\pm$ 0.001	0.084 $\pm$ 0.001
HD126614	14/01/2011	50000	0.179 $\pm$ 0.018	0.103 $\pm$ 0.005	0.090 $\pm$ 0.002	0.088 $\pm$ 0.002

**Table 5.** Average absolute magnitudes and ages of all target stars in an observation epoch

Epoch	MI [mag]	Age [Gyr]
23/04/2008	4.32	4.9
11/07/2008	3.43	6.0
16/01/2009	2.93	4.6
07/09/2009	2.64	6.2
23/02/2010	3.72	2.2
14/07/2010	4.14	7.4
14/01/2011	3.67	5.4
27/07/2011	3.20	6.5

at 2MASS Epoch May 3th 2000), the HD 126614 system is actually a hierarchical triple system, the only one presently known in which the planet host star exhibits a close stellar companion. All other known planet host triples are composed of the planet host star and a binary-companion at wider separation.

We also discovered one new low-mass ( $0.239 \pm 0.022 M_{\odot}$ ) stellar companion to the star HD 185269, with a separation of  $4.511 \pm 0.013$  arcsec at a position angle of  $8.44^{\circ} \pm 0.30^{\circ}$ . This corresponds to a projected distance of 227 AU. HD 185269A harbors a "Hot Jupiter" ( $M \sin i = 0.94 M_J$ ) with an orbital period of 6.8 d and a semi-major axis of 0.077 AU, detected by Johnson et al. (2006). They state that its orbital eccentricity of 0.3 is large in comparison with other planets found within 1 AU of their host stars. This could possibly be explained by the Kozai mechanism as described by Takeda and Rasio (2005). We used the formula

$$P \simeq 2\pi \sqrt{\frac{a_1^3}{G(m_0 + m_1)}} \left( \frac{m_0 + m_1}{m_2} \right) \left( \frac{a_2}{a_1} \right)^3 (1 - e_2^2)^{3/2}$$

to calculate the period of the Kozai oscillations (Ford et al. 2000), where the indices 0, 1 and 2 represent the host star, planetary and stellar companions respectively. Assuming an eccentricity of 0.5 for the stellar companion (as suggested by statistical analysis in Söderhjelm 1999), and a semi-major axis equal to the projected separation of 227 AU, we get a period of 1.7 Gyr. Given the age of HD 185269 A of 4.2 Gyr, this period is short enough so that the Kozai effect might

have altered the planetary companion's eccentricity and inclination.

For the remaining 66 target stars in our sample we can on average exclude all low-mass stellar companions of  $M > 0.15 M_{\odot}$  down to 2 arcsec around the primary. For many stars in our sample we get significantly deeper, enabling us to exclude all low-mass stellar companions outside of 2 arcsec and up to 12 arcsec. To further summarize our detection limits, in Fig. 14 we show the average dynamic range plot of all observations, with all detected stellar companions marked.

68 stars of our sample had an unknown multiplicity status before our observations. Of those, only one proved to be multiple within the detection limits of our survey. This yields a multiplicity rate of only 1.5 % for our sample. Given that the multiplicity rate of the known exoplanet host population is about 17 %, stellar multiple systems are underrepresented in our sample. However, since the sample size of our Astralux survey is not yet statistically significant ( $\geq 231$  for 95 % confidence level and an error margin of 5 %) we can not draw any conclusion for the whole exoplanet population. For a detailed statistical analysis of the properties of all known stellar multiple systems harboring extrasolar planets, we refer to Röll et al. (2011, submitted).

We will continue our current monitoring campaign in order to determine the multiplicity status of all exoplanet host stars, which then will yield the true multiplicity rate of planet-bearing stars. This will also eventually allow us to draw conclusions about the frequency of planets in multiple stellar systems, as well as their properties compared to planets which reside around single stars.

## ACKNOWLEDGMENTS

CG and TE wish to acknowledge Deutsche Forschungsgemeinschaft (DFG) for grant NE 515 / 30-1. MS would like to thank DFG for support in project NE 515 / 36-1. Based on observations collected at the Centro Astronómico Hispano Alemán (CAHA) at Calar Alto, operated jointly by the Max-Planck Institut für Astronomie and the Instituto de Astrofísica de Andalucía (CSIC). We would especially like

**Table 7.** List of all stars with no additional stellar components detected. We give the numbers of frames observed, each frame with an exposure time of 29.54 ms. We also give an upper limit for the minimum mass detectable at 0.5, 1, 2 and 5 arcsec using the models by Baraffe et al. (1998) and assuming an average age for each epoch as listed in Table 5.

Star	RA	DEC	Epoch	# of frames	M [ $M_{\odot}$ ] at 0.5''	M [ $M_{\odot}$ ] at 1''	M [ $M_{\odot}$ ] at 2''	M [ $M_{\odot}$ ] at 5''
HD 1461	00 18 41.8	-08 03 10.8	14/07/2010	55000	0.157 ± 0.011	0.099 ± 0.003	0.083 ± 0.001	0.082 ± 0.001
BD-1763	00 28 34.3	-16 13 34.8	07/09/2009	50000	0.110 ± 0.006	0.091 ± 0.003	0.083 ± 0.001	0.079 ± 0.001
Hat-P-19	00 38 04.0	+34 42 41.6	27/07/2011	50000	0.140 ± 0.022	0.109 ± 0.012	0.099 ± 0.008	0.098 ± 0.007
HD 4203	00 44 41.2	+20 26 56.1	11/07/2008	80000	0.176 ± 0.020	0.117 ± 0.008	0.091 ± 0.003	0.086 ± 0.002
HD 5319	00 55 01.4	+00 47 22.4	11/07/2008	50000	0.424 ± 0.047	0.221 ± 0.027	0.140 ± 0.013	0.128 ± 0.011
HIP 5158	01 06 02.0	-22 27 11.3	14/01/2011	50000	0.112 ± 0.008	0.089 ± 0.002	0.080 ± 0.002	0.079 ± 0.001
HD 6718	01 07 48.6	-08 14 01.3	14/01/2011	50000	0.211 ± 0.021	0.107 ± 0.005	0.085 ± 0.001	0.083 ± 0.001
HD 7924	01 21 59.1	+76 42 37.0	27/07/2011	50000	0.100 ± 0.003	0.082 ± 0.001	0.079 ± 0.001	0.078 ± 0.001
HD 8673	01 26 08.7	+34 34 46.9	14/01/2011	50000	0.270 ± 0.025	0.113 ± 0.006	0.089 ± 0.002	0.088 ± 0.001
HD 9446	01 33 20.1	+29 15 54.5	14/07/2010	55000	0.148 ± 0.011	0.099 ± 0.003	0.086 ± 0.001	0.083 ± 0.002
HD 16232	02 37 00.5	+24 38 49.9	23/02/2010	20000	0.402 ± 0.033	0.318 ± 0.034	0.208 ± 0.022	0.121 ± 0.007
HD 16175	02 37 01.9	+42 03 45.4	27/07/2011	50000	0.236 ± 0.024	0.108 ± 0.005	0.093 ± 0.003	0.091 ± 0.003
HD 16760	02 42 21.3	+38 37 07.2	23/02/2010	20000	0.289 ± 0.047	0.223 ± 0.036	0.159 ± 0.019	0.108 ± 0.009
HD 17092	02 46 22.1	+49 39 11.1	14/07/2010	55000	0.441 ± 0.181	0.213 ± 0.122	0.121 ± 0.043	0.112 ± 0.035
HIP 12961	02 46 42.8	-23 05 11.8	14/01/2011	50000	0.105 ± 0.004	0.077 ± 0.001	0.074 ± 0.001	0.074 ± 0.001
HD 17156	02 49 44.4	+71 45 11.6	23/02/2010	20000	0.465 ± 0.038	0.376 ± 0.038	0.243 ± 0.027	0.136 ± 0.010
HD 22781	03 40 49.5	+31 49 34.6	27/07/2011	50000	0.112 ± 0.005	0.086 ± 0.001	0.079 ± 0.001	0.078 ± 0.001
HD 28305 <sup>1</sup>	04 28 36.9	+19 10 49.5	07/09/2009	10000	0.862 ± 0.031	0.653 ± 0.028	0.342 ± 0.036	0.325 ± 0.034
HD 32518	05 09 36.7	+69 38 21.8	14/01/2011	50000	0.686 ± 0.036	0.259 ± 0.030	0.183 ± 0.020	0.185 ± 0.020
HD 34445	05 17 40.9	+07 21 12.0	14/01/2011	50000	0.219 ± 0.020	0.094 ± 0.003	0.089 ± 0.002	0.089 ± 0.002
HD 33564	05 22 33.5	+79 13 52.1	07/09/2009	50000	0.253 ± 0.022	0.148 ± 0.009	0.097 ± 0.003	0.095 ± 0.002
HD 38801	05 47 59.1	-08 19 39.7	14/01/2011	50000	0.363 ± 0.065	0.115 ± 0.012	0.097 ± 0.006	0.095 ± 0.005
HD 45652	06 29 13.2	+10 56 02.0	16/01/2009	22610	0.165 ± 0.013	0.118 ± 0.007	0.094 ± 0.003	0.087 ± 0.001
HD 45410	06 30 47.1	+58 09 45.4	14/01/2011	50000	0.474 ± 0.034	0.198 ± 0.019	0.127 ± 0.008	0.124 ± 0.007
HD 68988	08 18 22.1	+61 27 38.5	23/04/2008	50000	0.177 ± 0.015	0.120 ± 0.007	0.092 ± 0.003	0.084 ± 0.002
HD 73534	08 39 15.8	+12 57 37.3	14/01/2011	50000	0.287 ± 0.041	0.107 ± 0.007	0.093 ± 0.004	0.093 ± 0.003
HD 74156	08 42 25.1	+04 34 41.1	16/01/2009	16000	0.386 ± 0.040	0.216 ± 0.023	0.141 ± 0.011	0.131 ± 0.009
HD 75898	08 53 50.8	+33 03 24.5	23/04/2008	50000	0.222 ± 0.027	0.130 ± 0.010	0.096 ± 0.003	0.091 ± 0.003
HD 81688	09 28 39.9	+45 36 05.3	14/01/2011	48149	0.647 ± 0.032	0.291 ± 0.034	0.216 ± 0.024	0.216 ± 0.024
HD 87883	10 08 43.1	+34 14 32.1	14/01/2011	50000	0.107 ± 0.004	0.084 ± 0.001	0.078 ± 0.001	0.078 ± 0.001
HD 90043	10 23 28.3	-00 54 08.0	14/01/2011	50000	0.553 ± 0.032	0.183 ± 0.017	0.125 ± 0.008	0.126 ± 0.008
HIP 57050	11 41 44.6	+42 45 07.1	14/01/2011	50000	< 0.072	< 0.072	< 0.072	< 0.072
GJ 436	11 42 11.1	+26 42 23.7	11/07/2008	80000	0.080 ± 0.001	0.076 ± 0.001	0.073 ± 0.001	< 0.072
HD 104985	12 05 15.1	+76 54 20.6	16/01/2009	26480	0.682 ± 0.030	0.518 ± 0.034	0.253 ± 0.025	0.238 ± 0.023
HD 107148	12 19 13.5	-03 19 11.2	16/01/2009	50000	0.214 ± 0.021	0.147 ± 0.011	0.102 ± 0.004	0.090 ± 0.002
HD 109246	12 32 07.1	+74 29 22.3	14/01/2011	50000	0.157 ± 0.012	0.098 ± 0.003	0.087 ± 0.001	0.083 ± 0.001
HD 110014	12 39 14.7	-07 59 44.0	14/01/2011	50000	0.881 ± 0.041	0.534 ± 0.037	0.298 ± 0.037	0.287 ± 0.035
HD 114783	13 12 43.7	-02 15 54.1	23/04/2008	50000	0.125 ± 0.006	0.086 ± 0.001	0.078 ± 0.001	0.077 ± 0.001
HD 115617	13 18 24.3	-18 18 40.3	14/01/2011	50000	0.611 ± 0.025	0.354 ± 0.031	0.158 ± 0.011	0.155 ± 0.011
HD 118203	13 34 02.5	+53 43 42.7	23/04/2008	50000	0.249 ± 0.028	0.123 ± 0.008	0.096 ± 0.003	0.092 ± 0.003
HD 125612 A	14 20 53.5	-17 28 53.4	23/04/2008	50000	0.194 ± 0.021	0.130 ± 0.009	0.098 ± 0.003	0.087 ± 0.002
HD 128311	14 36 00.6	+09 44 47.4	14/01/2011	50000	0.106 ± 0.004	0.083 ± 0.001	0.077 ± 0.001	0.077 ± 0.001
HD 132406	14 56 54.7	+53 22 55.8	16/01/2009	32000	0.200 ± 0.021	0.139 ± 0.010	0.106 ± 0.005	0.093 ± 0.003
HD 136418	15 19 06.1	+41 43 59.5	27/07/2011	50000	0.463 ± 0.041	0.178 ± 0.017	0.109 ± 0.006	0.099 ± 0.004
HD 137759	15 24 55.7	+58 57 57.8	11/07/2008	60000	0.709 ± 0.026	0.467 ± 0.030	0.202 ± 0.017	0.191 ± 0.017
HD 142091	15 51 13.9	+35 39 26.6	16/01/2009	16000	0.549 ± 0.027	0.422 ± 0.033	0.233 ± 0.019	0.157 ± 0.011
HD 145675	16 10 24.3	+43 49 03.5	11/07/2008	80000	0.130 ± 0.007	0.098 ± 0.002	0.083 ± 0.001	0.081 ± 0.001
HD 148427	16 28 28.1	-13 23 58.6	14/07/2010	55000	0.371 ± 0.038	0.163 ± 0.013	0.098 ± 0.003	0.093 ± 0.003
HD 149026	16 30 29.6	+38 20 50.3	07/09/2009	50000	0.242 ± 0.025	0.128 ± 0.008	0.097 ± 0.003	0.092 ± 0.003
HD 150706	16 31 17.5	+79 47 23.2	07/09/2009	50000	0.160 ± 0.011	0.103 ± 0.004	0.086 ± 0.001	0.083 ± 0.001
HD 149143	16 32 51.0	+02 05 05.3	23/04/2008	50000	0.225 ± 0.023	0.103 ± 0.005	0.088 ± 0.002	0.087 ± 0.002
GL 649	16 58 08.8	+25 44 38.9	14/07/2010	40950	0.080 ± 0.001	0.074 ± 0.001	< 0.072	< 0.072
HD 154345	17 02 36.4	+47 04 54.7	07/09/2009	50000	0.139 ± 0.009	0.098 ± 0.003	0.083 ± 0.001	0.079 ± 0.001
HD 155358	17 09 34.6	+33 21 21.0	14/07/2010	53240	0.174 ± 0.013	0.101 ± 0.003	0.086 ± 0.001	0.085 ± 0.001
GJ 1214	17 15 18.9	+04 57 49.7	14/07/2010	55000	0.075 ± 0.001	< 0.072	< 0.072	< 0.072
HD 156668	17 17 40.4	+29 13 38.0	14/07/2010	55000	0.101 ± 0.003	0.086 ± 0.001	0.078 ± 0.001	0.077 ± 0.001
HD 164922	18 02 30.8	+26 18 46.8	07/09/2009	50000	0.133 ± 0.008	0.096 ± 0.003	0.082 ± 0.001	0.080 ± 0.001
HD 167042	18 10 31.6	+54 17 11.5	07/09/2009	50000	0.484 ± 0.028	0.256 ± 0.022	0.130 ± 0.008	0.108 ± 0.005
HD 170693	18 25 59.1	+65 33 48.5	14/07/2010	55000	0.764 ± 0.028	0.542 ± 0.029	0.279 ± 0.028	0.286 ± 0.031
HD 173416	18 43 36.1	+36 33 23.7	27/07/2011	50000	0.741 ± 0.033	0.419 ± 0.040	0.247 ± 0.027	0.242 ± 0.026
HD 188310	19 54 14.8	+08 27 41.2	07/09/2009	50000	0.667 ± 0.030	0.455 ± 0.039	0.187 ± 0.019	0.161 ± 0.014
HD 200964	21 06 39.8	+03 48 11.2	27/07/2011	50000	0.356 ± 0.040	0.144 ± 0.012	0.116 ± 0.007	0.112 ± 0.006
HD 218566	23 09 10.7	-02 15 38.6	27/07/2011	50000	0.107 ± 0.004	0.084 ± 0.001	0.079 ± 0.001	0.078 ± 0.001
HD 221345	23 31 17.4	+39 14 10.3	07/09/2009	50000	0.653 ± 0.028	0.365 ± 0.036	0.183 ± 0.017	0.169 ± 0.014

<sup>1</sup> the companion candidate (Mason et al. 2009) at 0.237 arcsec separation could not be resolved

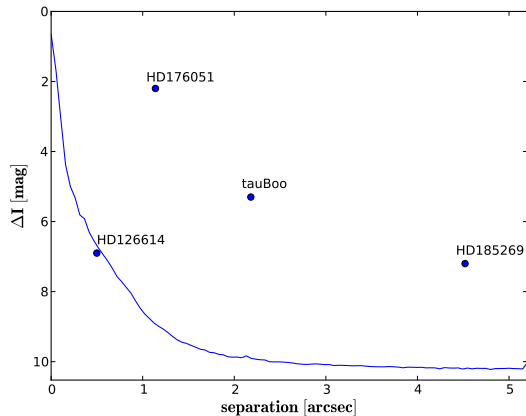


**Figure 14.** Average dynamic range in all observation epochs after PSF subtraction. All detected stellar companions have been added. The typical standard deviation is 0.2 mag.

to express our thanks to the very helpful staff at the Calar Alto observation site. We used Simbad and Vizier as well as archival data from HST. HST data were obtained from the data archive at the Space Telescope Institute, which is operated by the association of Universities for Research in Astronomy, Inc. under the NASA contract NAS 5-26555. This publication makes use of data products from the Two Micron All Sky Survey, which is a joint project of the University of Massachusetts and the Infrared Processing and Analysis Center/California Institute of Technology, funded by the National Aeronautics and Space Administration and the National Science Foundation. This research has made use of the Washington Double Star Catalog maintained at the U.S. Naval Observatory. We made use of the SciPy tools for scientific computation in Python by Jones et al. (2001–). CG would also like to express special thanks to Tristan Röll and Christian Adam for their invaluable help and comments regarding the Python programming language as well as Tobias Schmidt and Hiroshi Kobayashi for fruitful discussion. Finally, we would like to thank Donna Keeley for the language editing of our manuscript.

## REFERENCES

Baraffe, Chabrier, Allard, Hauschildt, 1998, *A&A*, 337, 403  
Bertin, E. and Arnouts, S., 1996, *A&A*, 117, 393  
Chauvin, G. and Beust, H. and Lagrange, A.-M. and Eggenberger, A., 2011, *A&A*, 528, 8  
Cutri, R. M. and Skrutskie, M. F. and van Dyk, S. and Beichman, C. A. and Carpenter, J. M. and Chester, T. and Cambresy, L. and Evans, T. and Fowler, J. and Gizis, J. and Howard, E. and Huchra, J. and Jarrett, T. and Kopan, E. L. and Kirkpatrick, J. D. and Light, R. M. and Marsh, K. A. and McCallon, H. and Schneider, S. and Stiening, R. and Sykes, M. and Weinberg, M. and Wheaton, W. A. and Wheelock, S. and Zacarias, N., 2003, 2MASS All-Sky Catalog of Point Sources (Cutri+ 2003), VizieR Online Data Catalog  
Daemgen, S. and Hormuth, F. and Brandner, W. and Bergfors, C. and Janson, M. and Hippler, S. and Henning, T., 2009, *A&A*, 498, 567  
Duchêne, G. and Delgado-Donate, E. and Haisch, Jr., K. E. and Loinard, L. and Rodríguez, L. F., 2007, *Protostars and Planets V*, 379  
Ford, E. B. and Kozinsky, B. and Rasio, F. A., 2000, *ApJ*, 535, 385  
Fukugita, M. and Ichikawa, T. and Gunn, J. E. and Doi, M. and Shimasaku, K. and Schneider, D. P., 1996, *AJ*, 111, 1748  
Hormuth, F., Diploma Thesis University of Heidelberg, 2007  
Hormuth, F. and Hippler, S. and Brandner, W. and Wagner, K. and Henning, T., 2008, *proceedings of the SPIE*, 7014, 138  
Howard, A. W. and Johnson, J. A. and Marcy, G. W. and Fischer, D. A. and Wright, J. T. and Bernat, D. and Henry, G. W. and Peek, K. M. G. and Isaacson, H. and Apps, K. and Endl, M. and Cochran, W. D. and Valenti, J. A. and Anderson, J. and Piskunov, N. E., 2010, *ApJ*, 721, 1467  
Johnson, J. A. and Marcy, G. W. and Fischer, D. A. and Henry, G. W. and Wright, J. T. and Isaacson, H. and McCarthy, C., 2006, *ApJ*, 652, 1724  
Jones, E. and Oliphant, T. and Peterson, P. and others, 2001–, SciPy: Open source scientific tools for Python, <http://www.scipy.org/>  
Lada, C. J., 2006, *ApJ*, 640, 63  
Law, N. M. and Mackay, C. D. and Baldwin, J. E., 2006, *A&A*, 446, 739  
van Leeuwen, F., 2007, "Hipparchos, the New Reduction of the Raw Data" *Astrophysics & Space Science Library* #350  
Mason, B. D. and Hartkopf, W. I. and Gies, D. R. and Henry, T. J. and Helsel, J. W., 2009, *AJ*, 137, 3358  
Mathieu, R. D. and Ghez, A. M. and Jensen, E. L. N. and Simon, M., 2000, *Protostars and Planets IV*, 703  
Mugrauer, M. and Seifahrt, A. and Neuhäuser, R., 2007, *MNRAS*, 378, 1328  
Mugrauer, M. and Neuhäuser, R., 2009, *A&A*, 494, 373  
Mutterspaugh, M. W. and Lane, B. F. and Kulkarni, S. R. and Konacki, M. and Burke, B. F. and Colavita, M. M. and Shao, M. and Hartkopf, W. I. and Boss, A. P. and Williamson, M., 2010, *AJ*, 140, 1657  
Patience, J. and White, R. J. and Ghez, A. M. and McCabe, C. and McLean, I. S. and Larkin, J. E. and Prato, L. and Kim, S. S. and Lloyd, J. P. and Liu, M. C. and Graham, J. R. and Macintosh, B. A. and Gavel, D. T. and Max, C. E. and Bauman, B. J. and Olivier, S. S. and Wizinowich, P. and Acton, D. S., 2002, *ApJ*, 581, 654  
Perryman, M. A. C. and Lindegren, L. and Kovalevsky, J. and Hoeg, E. and Bastian, U. and Bernacca, P. L. and Crézé, M. and Donati, F. and Grenon, M. and van Leeuwen, F. and van der Marel, H. and Mignard, F. and Murray, C. A. and Le Poole, R. S. and Schrijver, H. and Turon, C. and Arenou, F. and Froeschlé, M. and Petersen, C. S., 1997, *A&A*, 323, 49  
Roddier, F. and Gilli, J. M. and Lund, G., 1982, *JOpt*, 13, 263  
Röll, T. and Seifahrt, A. and Neuhäuser, R. and Köhler, R., 2011, *ASPC*, 435, 419  
Röll, T. and Seifahrt, A. and Neuhäuser, R. and Mugrauer,

R., 2011, A&A, submitted  
Sánchez, S. F. and Aceituno, J. and Thiele, U. and Pérez-  
Ramírez, D. and Alves, J., 2007, PASP, 119, 1186  
Schneider, J. and Dedieu, C. and Le Sidaner, P. and Savalle,  
R. and Zolotukhin, I., 2011, A&A, 532, 79  
Söderhjelm, S., 1999, A&A, 341, 121  
Takeda, G. and Rasio, F. A., 2005, ApJ, 627, 1001